Quasi-Geostrophic Diagnosis of the Monsoon Depression of 5–8 July 1979

FREDERICK SANDERS

Center for Meteorology and Physical Oceanography, Massachusetts Institute of Technology, Cambridge, MA 02139

(Manuscript received 1 August 1983, in final form 31 October 1983)

ABSTRACT

Quasi-geostrophic diagnosis of the fields of vertical motion and streamfunction tendency, based on wind analysis, was undertaken for the monsoon depression of 5–8 July 1979, a uniquely well-observed case during Summer MONEX. Wind analysis, in terms of streamfunction and velocity potential, was performed for data averaged in three layers of equal pressure depth from 1000 to 100 mb. The thermal stratification near the depression above 850 mb was approximately moist-adiabatic. The wind analyses showed that the basic zonal currents, westerly in the lower troposphere and easterly in the middle levels, weakened as the depression formed. Central vorticity increased rapidly on 5–6 July to a magnitude three times the Coriolis parameter. The center tilted toward the southwest with elevation.

The quasi-geostrophic omega-equation was solved at the interfaces between layers, for a range of stabilities from the full dry-adiabatic value to 1% of it. Ascent west of the center for the near-neutral stability was sufficient to account for the storm-scale average observed precipitation. Divergences for each layer were combined with vorticity advections to calculate the quasi-geostrophic streamfunction tendencies. The observed slow westward motion of the system was reasonably well accounted for, but the temporally increasing meridional slope of the system was somewhat exaggerated. The strong increase in central vorticity during development could not be accounted for by divergence arising from advections of temperature and vorticity.

1. Introduction

Monsoon depressions are cyclones with winds of moderate but rarely destructive strength which form during the summer season near the head of the Bay of Bengal. They are nearly stationary at first but then move toward the west-northwest at speeds up to about 5 m s^{-1}, crossing the Indian coast and losing their identity in the extensive zonal trough of low pressure over the northern part of the country. Storm paths are especially localized during July and August. The heavy precipitation which lies mainly west or southwest of the low center, and thus precedes its passage, constitutes an important part of the rainfall during the southwest monsoon season. Rao (1976) has presented a detailed climatology of the phenomenon.

These storms occur in a unique large-scale tropical environment. Nowhere else in low latitudes are mean zonal currents and vertical wind shear as strongly developed. The shear of 35 m s^{-1} between 850 and 200 mb (Fig. 1) is balanced geostrophically by a horizontal temperature gradient of 0.42 g K (100 km)$^{-1}$. Although monsoon depressions form poleward of the region of strongest vertical shear, where the effects of lateral shear are not to be discounted, the presence of substantial vertical shear implies the possible dynamical importance of temperature advection and differential vorticity advection. It is desirable to obtain a quantitative assessment of the importance of these mechanisms for the development of the depression, for its movement, and for its associated rainfall. In fact, Rao and Rajamani (1970) and Krishnamurti *et al.* (1976) have obtained at least qualitatively encouraging results in quasi-geostrophic models embodying these mechanisms.

As to development of the depression, Keshavamurty *et al.* (1978) have argued that baroclinic instability cannot be the mechanism, since the disturbance tilts toward the west with elevation, down the vertical shear of the zonal wind vector. This tilt was derived mainly from Indian data, taken for the most part during the mature or dying stages of the depression. Developmental conditions, in the Bay or near the Burmese coast, had been little observed. In the data shown by Keshavamurty *et al.* (1978, in their Fig. 5), in fact, the westerly wind at Port Blair (near 12 N, 93 E) veered with elevation, indicating an eastward, upshear tilt of this portion of the disturbance on the day of formation, introducing ambiguity into the picture.

Further doubt about the efficacy of baroclinic instability is raised by the case study of Raman *et al.* (1978), during the Indo–USSR Monsoon-77 Experiment. The vertical wind shear decreased over the upper Bay of Bengal and adjacent Indian coast shortly prior to depression development. The strong decreases were limited in area, however, and the shear increased dramatically in the southern part of the Bay so that the changes appear to have been associated with a distur-

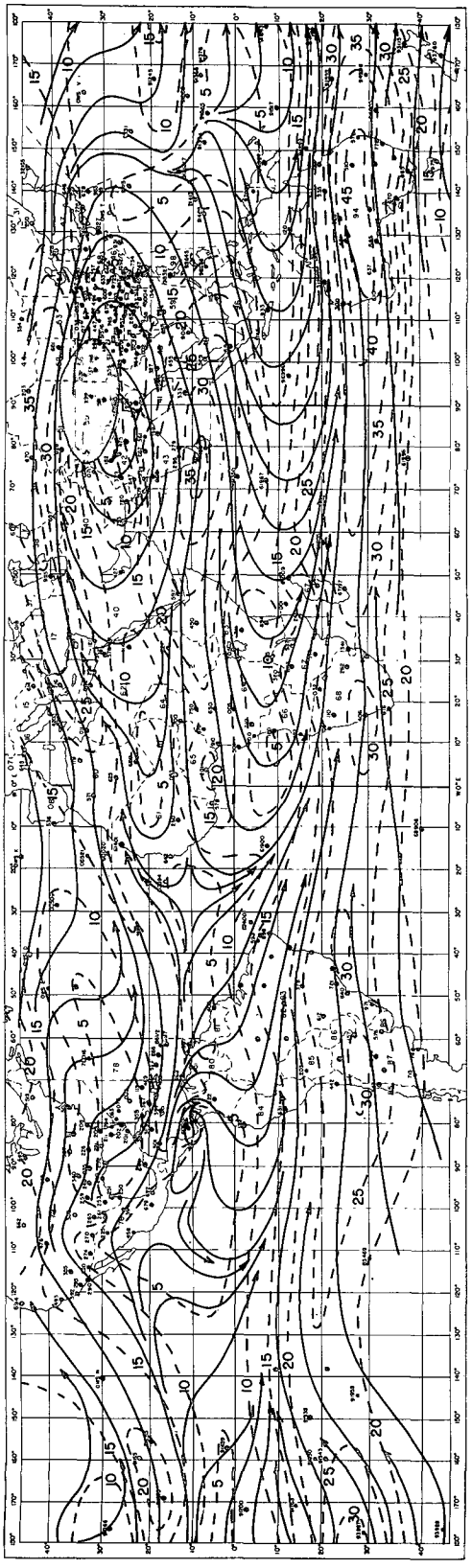

FIG. 1. Vertical wind shear from 850 to 200 mb during June–August. Adapted from Newell *et al.*, (1972). Dashed lines are isotachs of shear, labeled in meters per second.

bance of synoptic scale rather than with an altered base state which is germane to the baroclinic instability problem.

Whatever the mechanism of initiation and intensification may be, other aspects of storm behavior are likely to be accounted for at least qualitatively by the baroclinic processes represented in quasi-geostrophic theory, as found by Rao and Rajamani (1970). For example, depressions move slowly westward despite being embedded in a westerly current in the lower troposphere. Thus there must be absolute vorticity production west and destruction east of the cyclone center. But with an easterly thermal wind, warm and cold advection west and east of the center, respectively, would yield (from quasi-geostrophic theory) the convergence and divergence necessary for vorticity change. For example, warm advection west of the center would be associated with ascent, low-level convergence, and vorticity production. A similar mechanism with a westerly thermal wind is shown by Sanders (1971), among others, to be responsible for the eastward motion of cyclones in higher latitudes. The same argument also implies ascent and precipitation west of the monsoon depression, in agreement with observation, even though the rain is highly convective.

Working in other longitudes, Burpee (1972) found baroclinic effects to be important in the dynamics of African waves, westward-propagating disturbances embedded in a large-scale easterly thermal wind south of the Sahara, with some structural similarity to monsoon depressions. Altogether, it appears worthwhile to examine further the role played by baroclinic processes in these storms.

To proceed along these lines is not to deny the existence of cumulus convection nor to denigrate *a priori* its large-scale importance. If we find that some aspect of depression behavior is not even qualitatively accounted for by the effects of temperature and vorticity advection we measure, then the large-scale importance is clear. If the convection, however, is embedded in an atmosphere that is saturated, or nearly so, on the scale of the storm, then its effect may be only on the small-scale distributions of rainfall and other elements. These latter aspects are important but are not the subject of this investigation. The major goal of this investigation is to distinguish those aspects of storm behavior that depend directly and crucially on the bulk effects of cumulus convection from those that do not.

Our formulation will be a quasi-geostrophic one, despite lack of *a priori* justification due to low latitude, strong wind, and small effective static stability. The approach, therefore, is heuristic, based on success obtained in previous application in comparably unjustifiable circumstances.

2. The depression of July 1979

The monsoon depression of 5–8 July 1979 occurred during the summer MONEX field program and was

uniquely well observed, especially by numerous dropwindsondes from research aircraft over the Bay (WMO, 1981). Its motion and behavior appears to have been typical. During the first few days of the month there was weak evidence of a westward-moving upper-level trough over Southeast Asia, apparently acting as a predecessor of the depression, as Saha *et al.* (1981) found to be typical.

On 3 July, the aircraft and land-based upper-wind observations (Fig. 2) defined a trough oriented northeast–southwest from the middle of the Bay of Bengal to central Burma. This trough displayed little systematic vertical slope, being toward the west with elevation

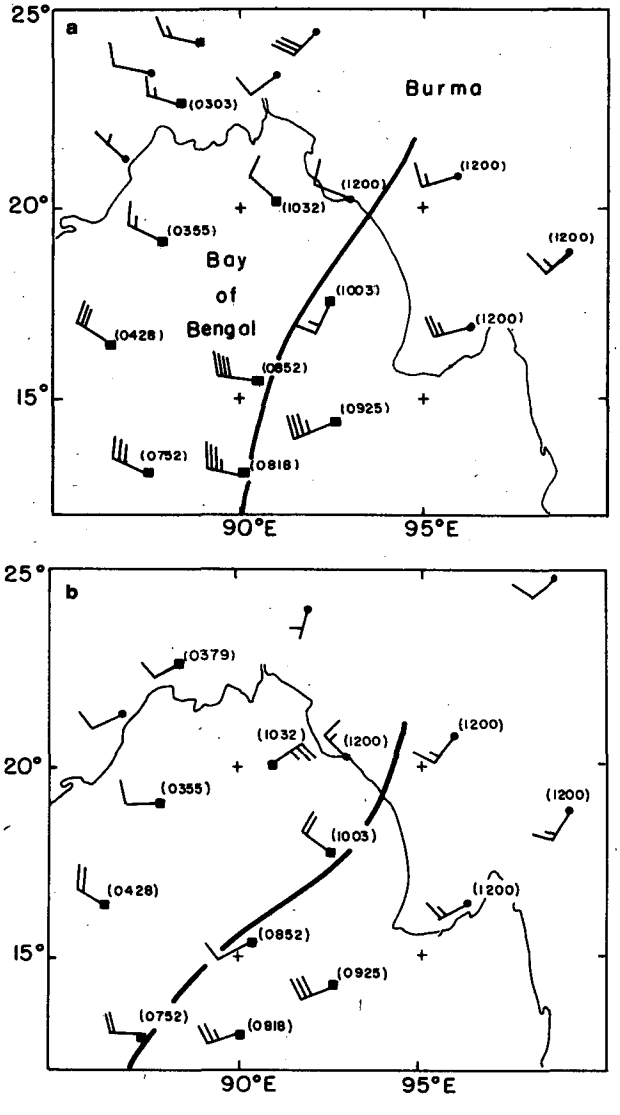

FIG. 2. Wind observations on 3 July: (a) at 850 mb and (b) at 500 mb. Time is 0000 GMT unless otherwise indicated in parentheses. Station circles represent rawinsonde data, squares dropwindsonde. The heavy line represents the trough as defined by the 270 deg isogon.

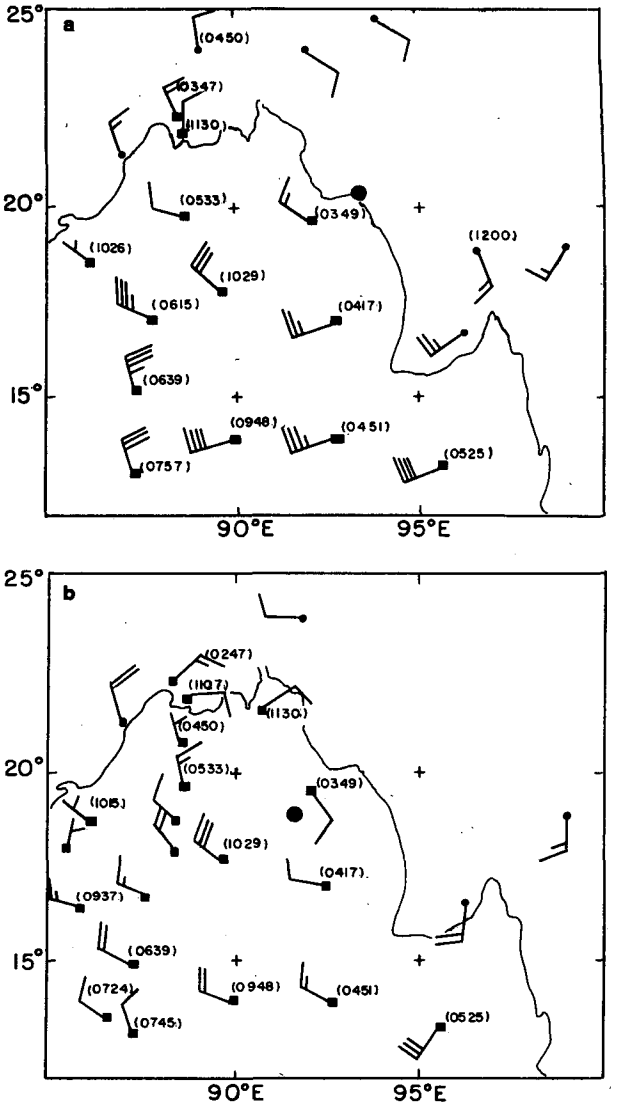

FIG. 3. As in Fig. 2 except for 5 July. Large dot represents the estimated position of the circulation center.

over the Bay and perhaps toward the east near the coast. The dropwindsondes nearest the coast, at 1003 and 1032 GMT, showed some possibly erroneous small-scale variability not seen in the Burmese soundings.

After an unfortunate gap in the aircraft observational program on 4 July, a weak circulation center was apparent on 5 July, as seen in Fig. 3, near the Burmese coast at 850 mb and over the Bay some 250 km to the southwest at 500 mb. The trough containing the center now sloped toward the west north of the center and toward the east south of it. The sharp, nearly 90 degree wind shift in the southwest portion of Fig. 3a had no temporal continuity and arises from observations by different aircraft. Those data west of 86°E are felt to be erroneous, as they show stronger merid-

ional components than observed at almost any other time or place. Warner (1984) has made a similar judgment.

By the next day the circulation had strengthened markedly at both levels (Fig. 4), with the center still sloping toward the southwest. A slow west-southwestward displacement of the system had begun, at a rate of about 2 m s^{-1}.

On 7 July (Fig. 5), there was some further intensification and the beginning of a separation of the lower-tropospheric center, moving westward at 3 m s^{-1}, from the midtropospheric center, which had progressed west-southwestward at 4 m s^{-1}. Warner (1984) also finds a southwestward tilt of the center with elevation on this day. On the 8th and 9th the system crossed the coast and weakened over the Indian peninsula, the 850 mb

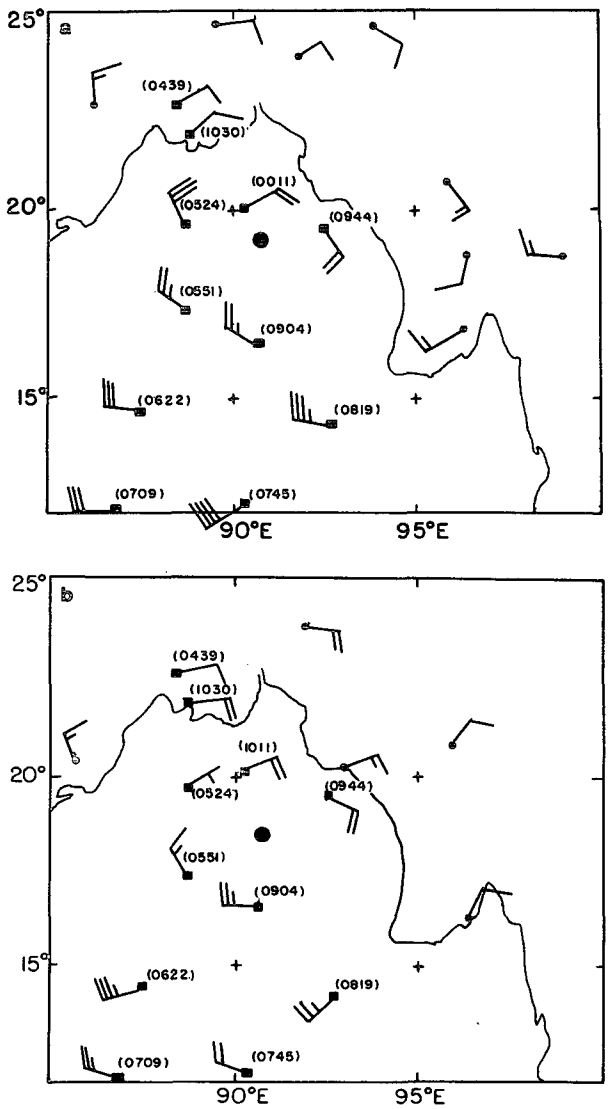

FIG. 4. As in Fig. 3 except for 6 July.

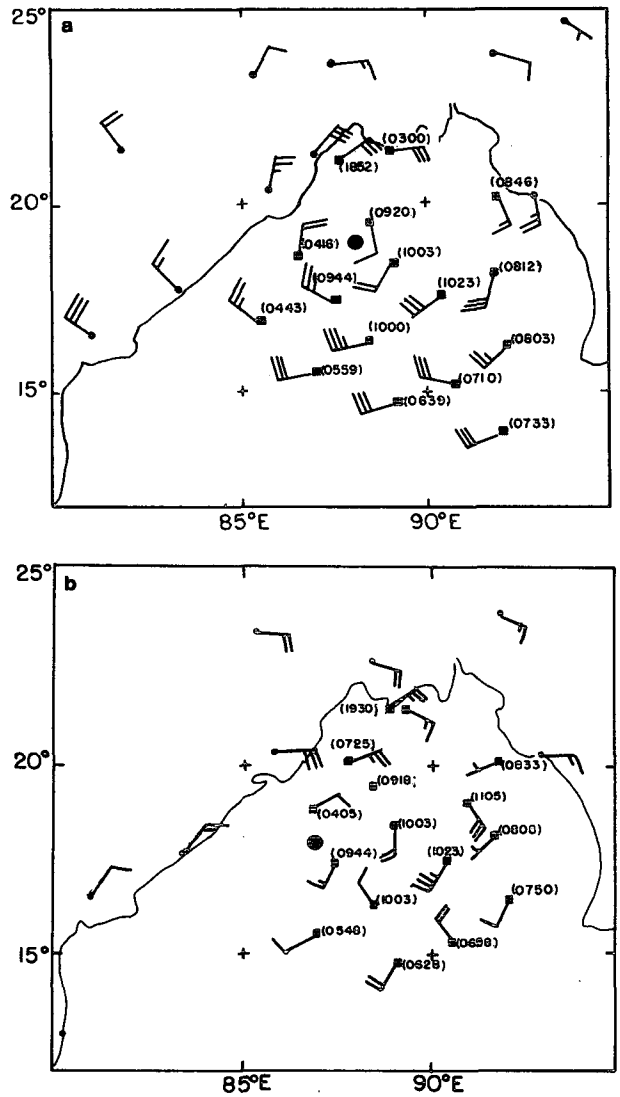

FIG. 5. As in Fig. 3 except for 7 July.

center moving northwestward and the 500 mb westward, both at about 5 m s^{-1}, so as to produce a substantial separation. The path is summarized in Fig. 6.

The available TIROS-N imagery, which was not of particularly high quality, showed great masses of cirrus cloud throughout most of the period, indicating (if due allowance was made for transport of cloud material by the strong upper-tropospheric easterlies) where convective or large-scale ascent was occurring, but obscuring much of the detail below. The visible and IR imageries at a given time were highly correlated. On the 3rd, the trough was embedded in an extensive region of deep cloud. Such striations as could be seen were largely zonal and not organized relative to the trough. As the circulation center formed and intensified on the 5th and 6th, cloud cleared from the area over the Bay north of the center, probably as a consequence

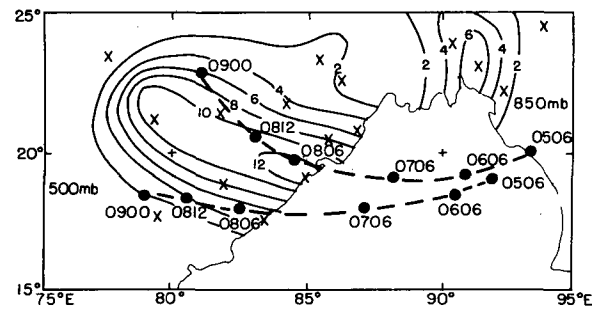

FIG. 6. Path of the depression center and total precipitation, 5–9 July. The date and GMT of each position are indicated by the 4-digit group. Precipitation data begin and end at 0300 GMT. Isohyets are labeled in centimeters. Stations reporting precipitation are shown by Xs.

of topographic descent in the developing easterly flow at low levels. There was little evidence of cloud suppression upshear (east) from the center as might be expected from quasi-geostrophic theory, since cold advection should be associated with subsidence. At this time and place, however, low-level southwesterlies (Fig. 3a and 4a) were impinging on the rugged Burmese coast with convection initiated by topographic lifting. Only on the 7th did cloudiness diminish over the Bay as the system moved westward toward the Indian coast. By that time, low-level winds (Fig. 5a) were nearly parallel to the Burmese coast. On the 8th, there was a clear distinction between extensive cloud west of the disturbance over India and relatively cloudless conditions over the Bay to the east of the system. At no time was there a "vortex signature" of the type that characterizes satellite pictures of other intense cyclones in or out of the tropics. The total rainfall for the storm, derived from measurements at rather few stations, appears in Fig. 6. The swath of heaviest amounts from the coast into central India lay between the paths of the 850 and 500 mb centers, favoring the former. On the coast, substantial precipitation began after 0300 GMT on the 6th and ended by 0300 GMT of the 8th as the depression center passed inland. The separate area of rainfall extending northward from the head of the Bay was highly sporadic, but did not occur during the period of pronounced low-level easterly flow on the 5th and 6th when topographic descent was an effective inhibitor.

In summary, these are the facts for which we call on the baroclinic processes of temperature advection and differential vorticity advection (as expressed in quasi-geostrophic theory) to explain the growth of a substantial cyclonic circulation, its westward motion and increasing vertical slope toward the southwest, and the associated major cloud and precipitation areas west of the disturbance (discounting major topographic effects).

3. Methods of analysis

Owing to the generally low signal-to-noise ratio in the upper-level temperature and height data in the subtropics, it seemed preferable to base the diagnostic calculations on observations of wind rather than of pressure–height. A wind sounding, however, responds to high-frequency oscillations of smaller scale than the synoptic-scale features of interest. Serious aliasing of the latter can thus occur.

To mitigate this effect, Sanders and Burpee (1968) successfully applied wind data, pressure-averaged for a single layer through the depth of the troposphere, to the problem of hurricane track prediction. To capture the baroclinic effects of interest in the present problem would require, of course, mean winds for at least two layers. Since monsoon depressions are generally held to be most intense near the 700 mb level (e.g., Keshavamurty *et al.*, 1978), the patterns of wind shear and temperature gradient in the lower and upper troposphere may be importantly different. Hence for this investigation the wind observations were averaged over three layers of equal pressure depth extending from 1000 to 100 mb.

First, the wind data were averaged for a nominal time of 1200 GMT on 5, 6 and 7 July for lower, middle, and upper tropospheric layers 1000–700, 700–400, and 400–100 mb, over the area shown in Fig. 7. For rawinsondes the mandatory-level data were appropriately averaged for each layer. Dropwindsonde data over the Bay were available at each 50 mb up to ~400, for various times up to six hours or so from the nominal time of the analysis. The locations of these observations were adjusted on the basis of displacement of the depression center. When a few data were missing in a given layer, interpolation or extrapolation was used. If fewer than half the required data were present, no average was calculated for the layer.

Topography was treated more crudely than would be acceptable in a prediction model; the extreme gradient along the edges of the Tibetan plateau (Fig. 7) was considered to represent a vertical wall extending to the 700 mb level, along the 700 mb isobar. At stations and grid points within the plateau, the surface was presumed to be at 700 mb, and a calm wind was assigned to the lower layer. Elsewhere the surface pressure was assumed to be at 1000 mb for the purpose of wind analysis. The entire development occurred well to the south of the Himalayan slope where winds remained light throughout.

Manual analysis of the wind field was then performed in terms of isogons and isotachs for each of the three layers; an example appears in Fig. 8. Little smoothing was undertaken, in anticipation that further processing would damp or remove small-scale or spurious features. In some areas of little or no rawinsonde or dropsonde coverage, qualitative reference was made

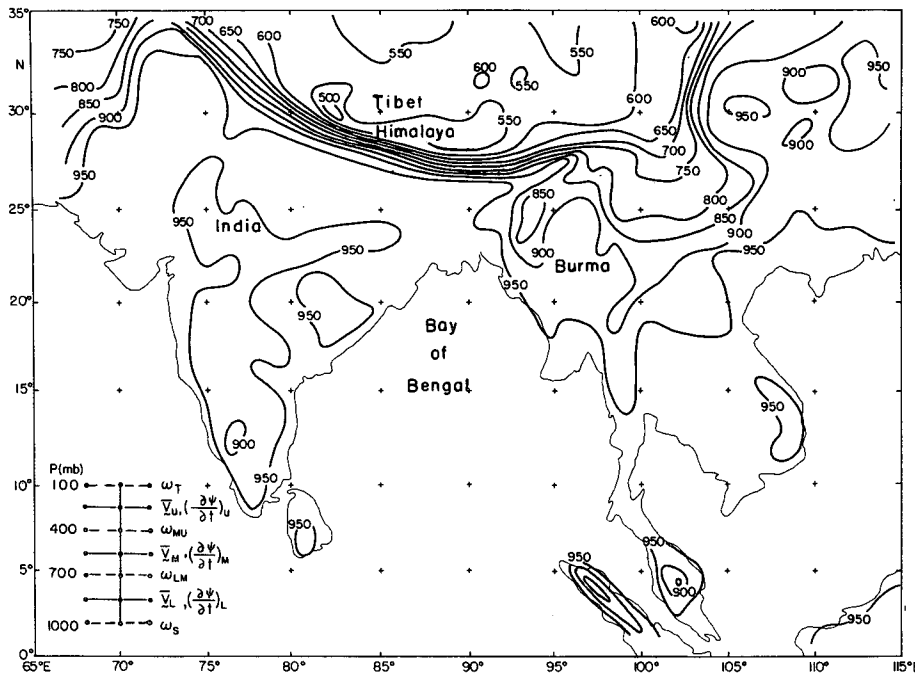

FIG. 7. The analysis and computational area, covered by a 34 × 26 grid with mesh length 1.5° longitude (154 km at 20°N). Solid lines represent surface pressure, labeled in millibar, obtained from the standard monsoon atmosphere of Saha and Singh (1972) and the 1° × 1° mean elevation data of Gates and Nelson (1975). The inset shows the vertical and horizontal grid.

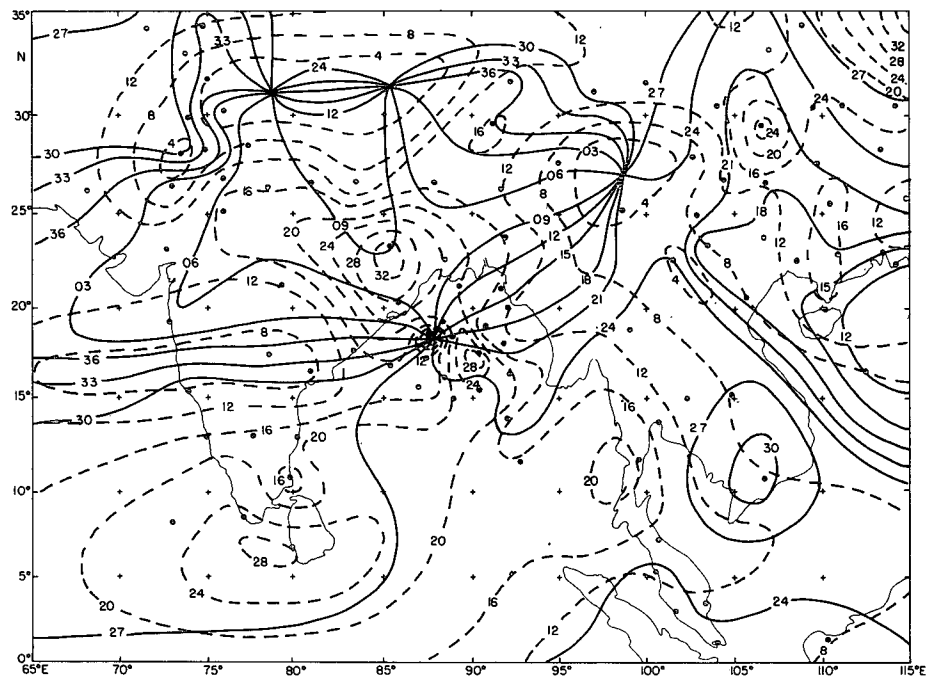

FIG. 8. Isogons (solid) at intervals of 30°, and isotachs (dashed) at intervals of 4 kt (1 kt = 0.52 m s^{-1}) for middle-layer mean winds at 1200 GMT 7 July. Dots indicate wind soundings.

to the analyses by Young *et al.* (1980) of satellite cloud-motion vectors. Data were especially sparse in the uppermost layer, but it appeared that there was little trace of the depression, to judge from the much weakened circulation at the top of the dropwindsondes near 400 mb and from the lack of systematic disturbance in the high cloud-motion vectors.

The next step was calculation of streamfunction (ψ) and velocity-potential (χ) fields from the vorticity and divergence, respectively, of the analyzed wind fields. To yield maximum kinetic energy of the nondivergent wind, represented by the streamfunction, the Neumann boundary condition, derived from the tangential component of the analyzed wind, was applied at the horizontal boundaries. For the velocity potential, it was assumed that the tangential component of the irrotational wind was zero.

The streamfunction fields had decidedly greater character than the velocity-potential fields, as confirmed by the data in Table 1. The former displayed ranges from maximum to minimum to more than 10 times greater than the latter. Peak nondivergent wind components were about three times their irrotational counterparts and were on a much larger scale. Generally, the velocity-potential fields displayed inflow over the region as a whole in the lower layer and outflow in the upper, consistent with average ascent. The details did not match the weather patterns, however, and no further use was made of the kinematic velocity potential.

4. Kinematic structure

Fields of streamfunction and absolute vorticity for the central portion of the computational domain appear in parts (a) and (c) of Figs. 9, 10 and 11. Comparison of streamfunction along the northern and southern boundaries shows in the middle layer a decrease in the area-averaged westerly component from 4.8 m s^{-1} on the 5th to 2.1 m s^{-1} and 2.0 m s^{-1} on succeeding days. In the lower layer there was a less dramatic decrease, from 5.9 m s^{-1} to 4.1 m s^{-1} over the 3 day period. These changes suggest a kinetic-energy conversion from basic current to disturbance, consistent with viewing depression development as a manifestation of barotropic-baroclinic instability, as suggested by Keshavamurty *et al.*, (1978).

TABLE 1. Characteristics of the fields of streamfunction and velocity potential

Layer	Total range (10^6 m^2 s^{-1})			Largest zonal or meridional component (m s^{-1})		
			ψ			
	5th	*6th*	*7th*	*5th*	*6th*	*7th*
Upper	44.9	45.1	42.4	23.9	22.3	23.2
Middle	29.2	23.5	22.0	13.0	13.2	14.3
Lower	32.3	29.7	26.2	16.5	18.0	15.6
			χ			
	5th	*6th*	*7th*	*5th*	*6th*	*7th*
Upper	3.5	9.8	7.3	5.1	5.9	7.5
Middle	2.5	3.2	3.6	3.2	4.4	5.3
Lower	3.9	5.0	4.5	5.8	6.6	5.2

The intensity of the growing disturbance must have arisen from another source, however, as the central absolute vorticity increased in the lower layer by a factor of 2, and in the middle layer by 60%, between the 5th and 7th. The greatest increase was from the 5th to the 6th, when a growth of lower-layer relative vorticity from 48 to 130 ($\times 10^{-6}$ s^{-1}) (roughly from 1 to 3 times the local value of f) occurred. In the middle layer, central relative vorticity rose from 61 to 102 ($\times 10^{-6}$ s^{-1}) in the same 24 h period. The important intensification occurred very rapidly, most strongly in the lower troposphere.

Close examination of the patterns on the 5th and 6th suggests that the southwestward displacement of the lower-layer streamfunction minimum represented a response to intensification in a westward-moving vorticity maximum. The southeastward displacement of the middle-layer vorticity maximum may represent the effect of upward transport of vorticity from the developing lower-layer disturbance.

Parts (b) and (d) of Figs. 9, 10 and 11 show the streamfunction fields, together with the differences between layers, representing under the quasi-geostrophic assumption both the vertical wind shear and the gradients of mean temperature between midpoints of layers. The temperature gradient is obtained by an appropriate form of the thermal-wind relationship

$$\nabla \bar{T} = \frac{f\bar{p}}{R} \nabla \frac{\Delta_p \psi}{\Delta p}, \qquad (1)$$

whence 15×10^5 m^2 s^{-1} − isopleths of $\Delta_p \psi$, the difference of ψ in this case from the lower to the middle layers represent, at 18°N, mean isotherms at intervals of 0.5°C. Similarly, the isopleths at intervals of 30×10^5 m^2 s^{-1} between middle and upper layers represent mean isotherms at intervals of 0.6°C. The substantial difference between the upper and lower temperature fields supports the use of more than two layers to represent the wind field.

On the 5th, the temperature structure in the lower to middle troposphere was ill-defined near the nascent disturbance center. Slightly cooler air lay to the west and warmer air to the east of the center. In the middle to upper troposphere the disturbance was characterized by a weak warm core at the northern edge of a relatively strong meridional temperature gradient. On the 6th, the intensification of the depression had been accompanied by an organization of lower temperature field comprising a systematic meridional gradient and a continuing zonal perturbation, colder to the west and

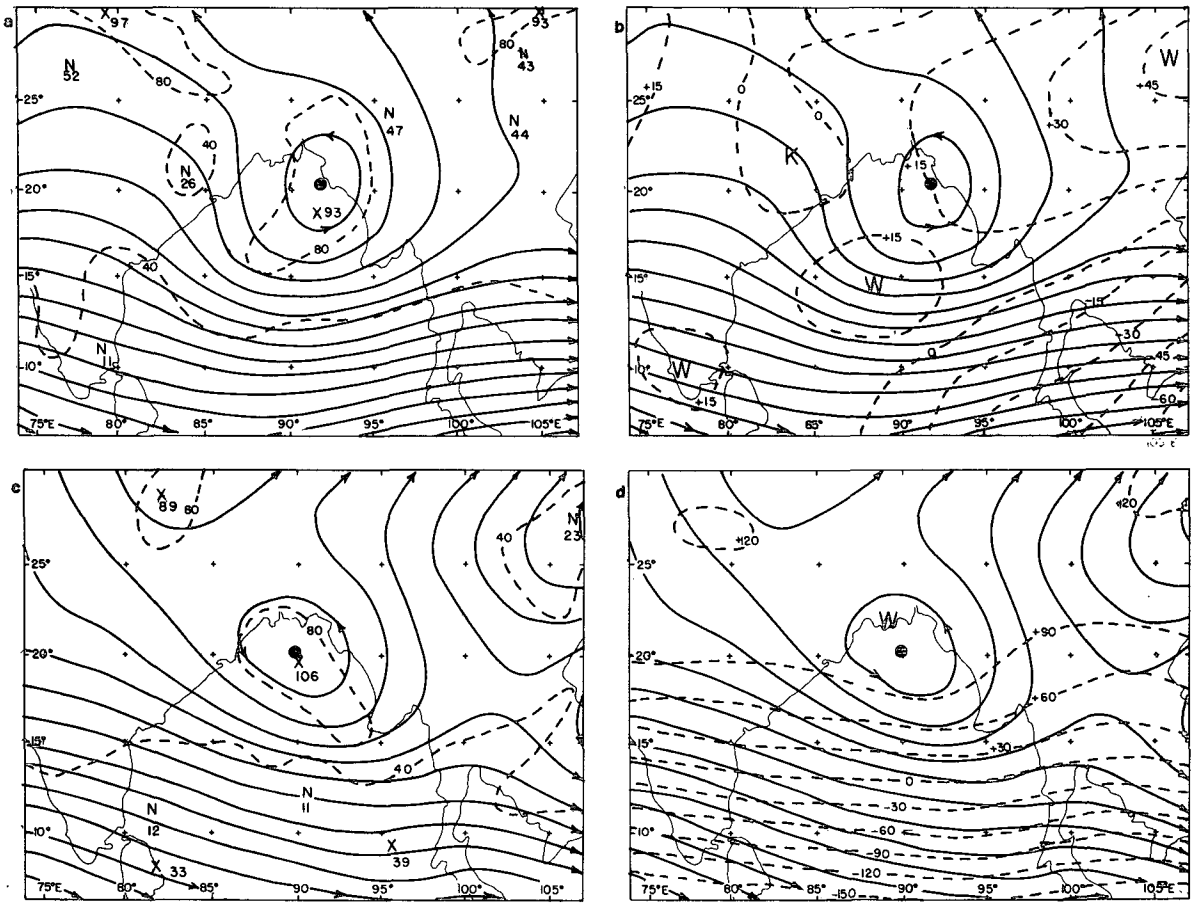

FIG. 9. At 1200 GMT 5 July: (a) lower-level streamfunction (solid) and absolute vorticity (dashed); (b) streamfunction at lower level and difference, middle minus lower levels (dashed); (c) middle-level streamfunction (solid) and absolute vorticity (dashed); and (d) streamfunction at middle levels and difference, upper minus middle levels (dashed). Streamfunction isopleths are at intervals of 15×10^5 m^2 s^{-1} with centers indicated by large dots. Vorticity isopleths are at intervals of 40×10^{-6} s^{-1}, with minima and maxima denoted by N's and X's, respectively, and by the extreme value. Isopleths of streamfunction difference are at intervals of 15×10^5 m^2 s^{-1} in (b) and of 30×10^5 m^2 s^{-1} in (d). These represent isotherms of mean temperature between (b) 850 mb and 550 mb and between (d) 550 mb and 250 mb at intervals of approximately 0.5°C and 0.6°C, respectively. Maxima and minima are labeled W and K.

warmer to the east of the center. In the upper temperature patterns, there was relatively little change. At both high and low levels, the patterns on the 7th resembled those of the 6th in their major aspects.

5. Vertical motion

With the streamfunction defined by $\psi \equiv gz/f_0$, where z is the height of a constant pressure surface and f_0 the value of the Coriolis parameter at 18°N, the quasi-geostrophic omega-equation can be written

$$\left[\sigma\nabla^2 + f_0^2\frac{\partial^2}{\partial p^2}\right]\omega = f_0\frac{\partial}{\partial p}\left[\mathbf{V}\cdot\nabla(\zeta + f)\right] - f_0\nabla^2\left(\mathbf{V}\cdot\nabla\frac{\partial\psi}{\partial p}\right) + f_0\nabla^2 Q + f_0\frac{\partial}{\partial p}(\nabla\times\mathbb{F}). \quad (2)$$

Here the wind is given by $\mathbf{V} = \mathbf{k}\times\nabla\psi$, the relative vorticity by $\nabla\times\mathbf{V} = \zeta = \nabla^2\psi$, ω is the "vertical" p-velocity dp/dt, σ is a measure of static stability $(\partial\ln\theta/\partial p)(g\partial z/\partial p)$, a horizontal average varying only with pressure, and Q is the change of $\partial\psi/\partial p$ due to diabatic heating. We did not attempt to represent Q explicitly, although an estimate of its importance was obtained implicitly, as we shall see, through use of an altered effective static stability. A friction force $\mathbb{F}$ may arise either from surface stress or from internal small-scale momentum transfers such as those possibly important ones which may be produced by cumulus convection. No attempt was made to evaluate $\mathbb{F}$, except in the lower boundary condition.

A finite difference analogue of (2) was solved on a 34×26 horizontal grid over the area shown in Fig. 7, with vertical resolution illustrated in the insert; that is, ω was obtained at 700 and 400 mb, the interfaces between layers. The upper and lateral boundary conditions were $\omega_s = 0$. At the lower boundary, calculations both with $\omega_s = 0$ and with

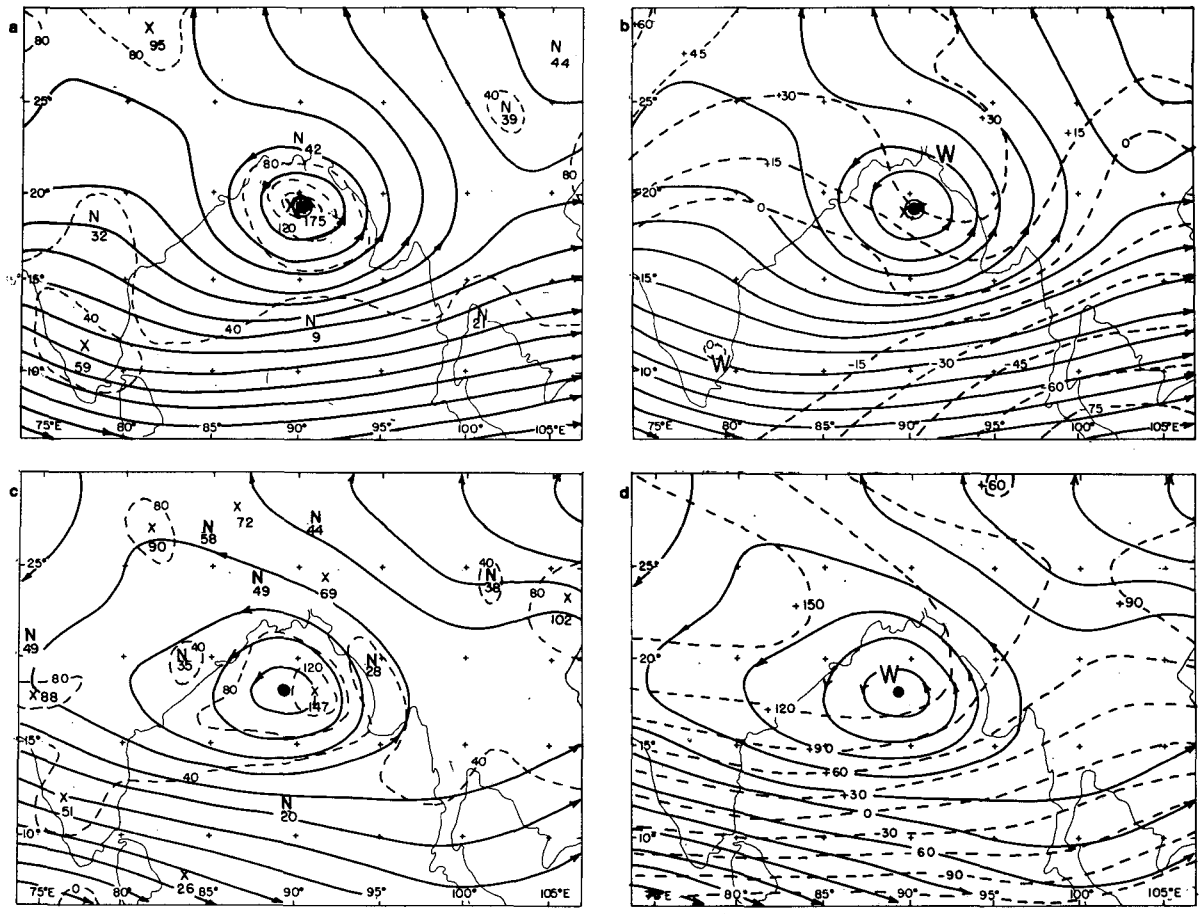

FIG. 10. As in Fig. 9 except at 1200 GMT 6 July.

$$\omega_s = \mathbf{V}_L \cdot \nabla p_s - (g/f_0)\mathbf{k} \cdot \nabla \times \rho_s c_D V_L \mathbf{V}_L \qquad (3)$$

where $\mathbf{V}_L$ is the mean wind in the lowest layer, p_s is the surface pressure mapped in Fig. 7, and c_D is the drag coefficient; that is, the vertical motion at the lower boundary was taken as the sum of effects due to topography and to Ekman pumping. In this equation it would be preferable to use the surface wind and to apply the lower boundary condition at an elevation of, say, one kilometer above the surface, rather than at the 1000 mb level. In the event, however, we found that this lower boundary condition had no salutary effect, nor was it especially large except in the lowest level. There seemed little point, therefore, in parameterizing the surface wind in terms of $\mathbf{V}_L$ or otherwise.

The static-stability parameter was obtained from a mean sounding (Fig. 12), representing an average of 1200 GMT coastal rawinsondes around the periphery of the Bay and dropwindsondes within it on 6 July. Data on the other days did not appear to indicate markedly different temperature and moisture structure. On the whole, substantial conditional instability was present only from the surface to 700 mb, owing to warm late afternoon temperatures at coastal locations. (The dropwindsonde data rarely reached below 930 mb or above 400 mb.) Near the center of the depression, the aircraft data showed virtually saturated air from 850–500 mb, relatively cool at the lowest level and warm aloft, with nearly neutral conditional stability.

The stability in the layer from 700 to 400 mb was deemed most important for this study, as the largest values of vertical motion would be expected in the middle troposphere. In an unsaturated thermodynamic process, the sounding shown in Fig. 12 yielded $\sigma = 3.65 \times 10^{-6}$ kg^{-2} s^2 for this layer. For a saturated process, however, σ was effectively zero. For comparative purposes, therefore, a number of values was used, ranging from the unsaturated value to 1% of it. The use of a stability smaller than the unsaturated value is a way of representing the effects of the release of latent heat of condensation of water vapor. This heating at a point is taken as proportional to the local value of the product of ω times the lapse rate of the saturation specific humidity along a moist adiabat. This way of representing the heating (or cooling) is appropriate when the atmosphere is in fact saturated on the scale on which ω is measured. Then the stability is obtained

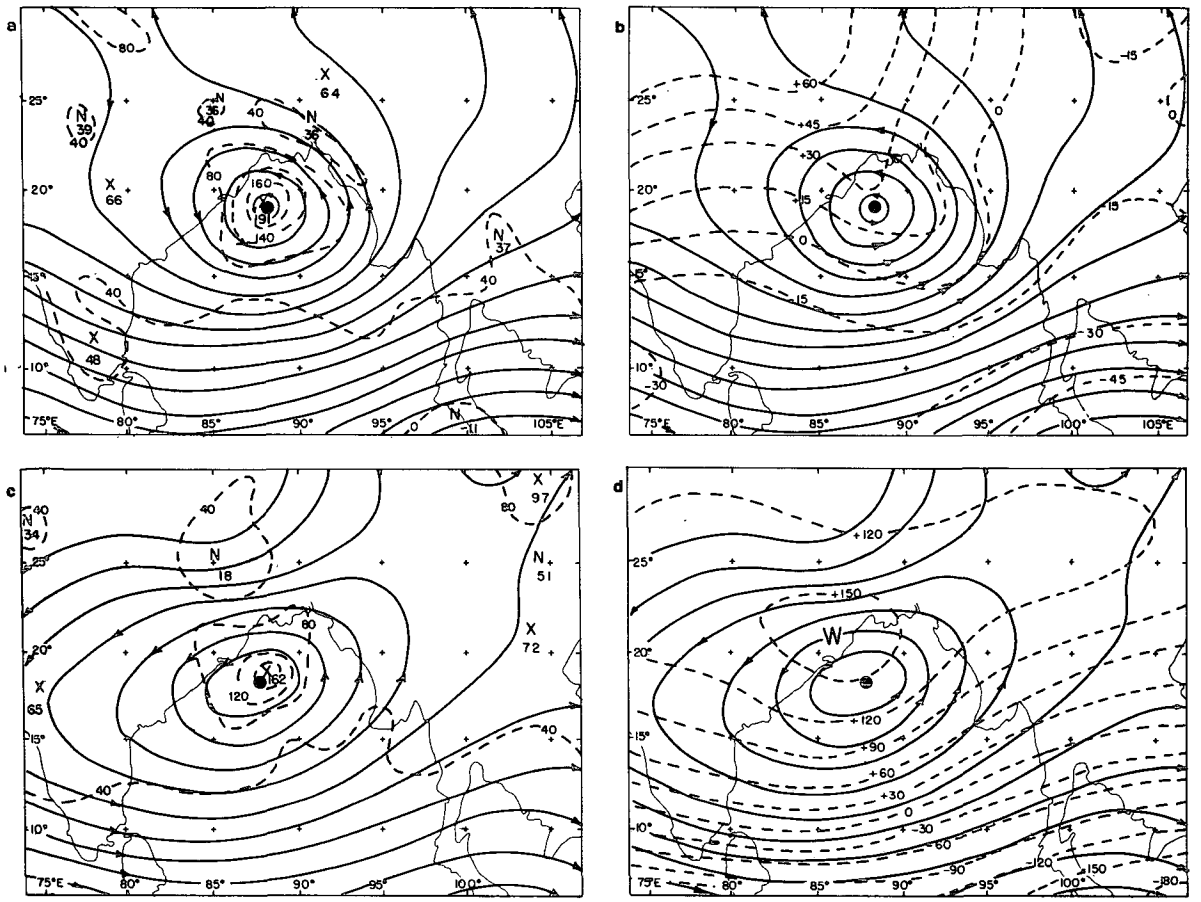

FIG. 11. As in Fig. 9 except at 1200 GMT 7 July.

by comparing the vertical temperature gradient with the moist-adiabatic lapse rate, yielding a value always smaller than the unsaturated one. In the present case the atmosphere is saturated or nearly so over much of the storm area, and the effective stability thus obtained is nearly zero. Where the atmosphere is not saturated, of course, the effective stability is the unsaturated value, and the use of a reduced value will exaggerate the vertical motion.

The results for vanishing ω_s showed that with unsaturated stability the vertical motions were extremely small, the maximum ascent associated with the depression never exceeding 3×10^{-4} mb s^{-1}, as Charney (1963) anticipated for tropical systems. With the 1% stability value simulating the effect of saturated conditions, vertical motions in this ascent region were about 30 times more intense and displayed much more small-scale character, consistent with the early arguments of Sumner (1950) and with numerous subsequent calculations. In the depression-associated ascent region, calculation of ω_s from Eq. (3) showed relatively little effect on vertical motion at higher levels. With the small stability, after the intensification of the depression, the enhancement over the values previously cited was ~10 and 3% at 700 mb and 400 mb, respectively. With larger, unsaturated, stability the ascent was about 40 and 10% greater at the two levels than values obtained with vanishing ω_s; fields of vertical motion for the 1% stability value and for vanishing ω at the lower boundary appear in Figs. 13, 14 and 15.

On 5 July (Fig. 13), the fields were not well organized with respect to the depression, although ascent northwest and descent southeast of the center was present at both levels. In the satellite imagery a few hours after the time of the calculation, large cloud clusters are seen in the region of weak ascent west of the center, but the main regions of extensive cloudiness occurred in weak to moderate ascent covering the southeast portion of the map area and in advance of a tropical storm approaching the coast from the South China Sea. On the whole, there was reasonable correspondence between regions of ascent and regions of extensive continuous high cloud. The only prominent exception was the ascent centered near 11°N, 84°E. The forcing here was due mainly to cyclonic vorticity advection in the upper troposphere, where the flow pattern was least reliably known. Of course, with unsaturated air these vertical motions are greatly overesti-

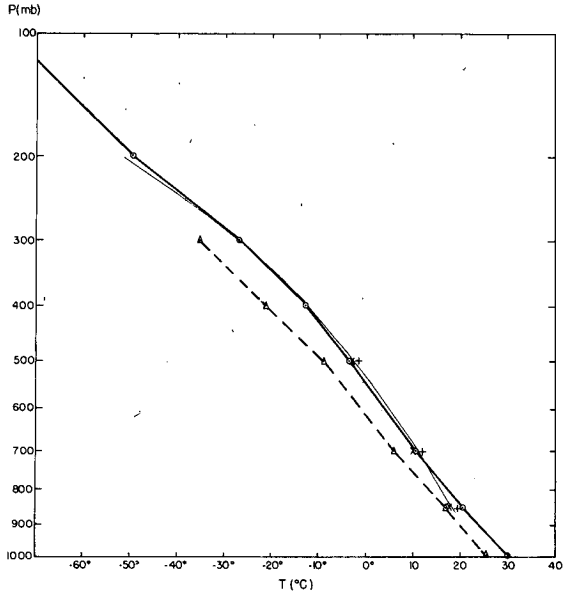

FIG. 12. Mean sounding of temperature (heavy solid) and dewpoint temperature (heavy dashed) for observations in the Bay of Bengal and surrounding coast on 6 July. The +s and Xs represent the mean of four dropwindsondes nearest the depression center. The thin solid line is a moist adiabat through the lifting condensation level of the 850 mb sample near the center.

mated. Nitta and Masuda's (1981) and Warner's (1984) patterns of subsidence are regarded as more reliable, although their kinematic methods are sensitive to smaller scales.

A day later (Fig. 14), there was a prominent doublet of ascent west and descent east of the intensified depression center. Major cloudiness accompanied the ascent and impinged on the descent region. The cloud mass associated with the tropical storm had moved inland in southern China along with the associated area of ascent; both were weakening.

On the 7th, the strong doublet still dominated the fields displayed in Fig. 15 (except for the small region of intense ascent near 12°N, 92°E, which was due to a 60-deg error in the input wind direction at a single grid point, detected after the computation had been completed). The eastern edge of the cloud mass associated with the depression now lay near the point of maximum ascent but no doubt extended farther eastward at 1200 GMT, the time of the calculation. Extensive cloudiness occurred in the region of general ascent over the southeastern portion of the map area, as on the two preceding days.

At both levels and on all three days, the depression center fell almost exactly on the zero-isopleth of vertical motion. Since ω was zero also at the base and top of the computational domain, the divergence over the center was almost exactly zero, and the model would not be expected to account for the intensification of the depression. This result characterized calculations with all the selected values of static stability. With nonzero values of ω_s, large divergence was calculated over the center.

Finally, it is interesting to calculate the condensation rate implied by the maximum diagnostic ascent on the 7th, as the depression crossed the Indian coast. Assume that the condensation rate is given by the product of ω and the rate of change of saturation mixing ratio along a moist adiabat, that the temperature structure is as given in Fig. 12 and that ω varies linearly from zero at 1000 mb to -99×10^{-4} mb s^{-1} at 700 mb to -57×10^{-4} mb s^{-1} at 400 mb to zero at 100 mb; then the integrated condensation rate is 1.18×10^{-4} gm s^{-1}. Expressed as a rainfall rate at the ground, this value would yield 0.43 cm h^{-1} or 10.2 cm day^{-1}. This rate compares favorably with the total rainfall along the path of the depression, shown in Fig. 6, given that the storm probably lasted more than 24 h at a given point but, of course, at less than the computed peak rate.

Convective activity may have been embedded within the large-scale cloud mass, but it is easily shown that

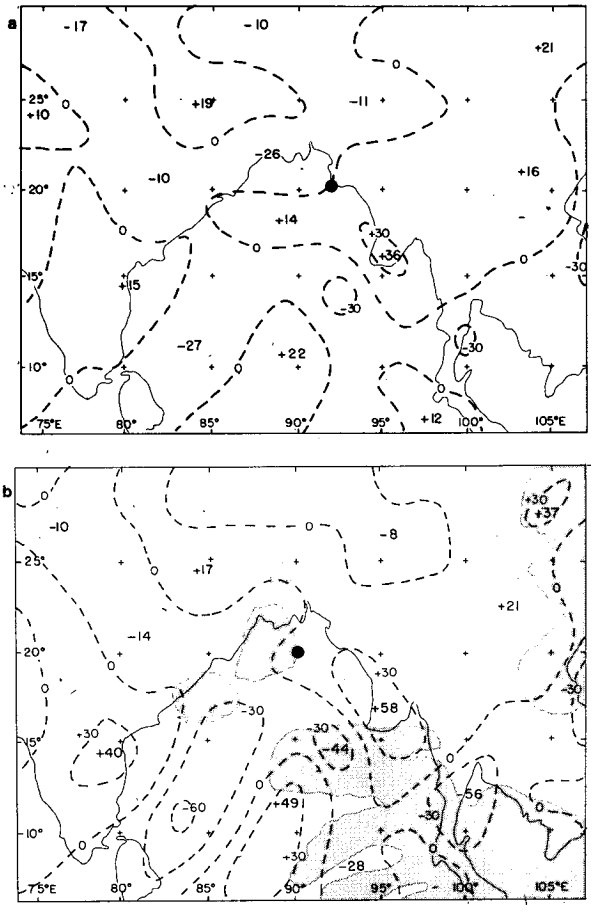

FIG. 13. "Vertical" motion ω (10^{-4} mb s^{-1}), at 1200 GMT 5 July: (a) at 700 mb, (b) at 400 mb. Large dot denotes the position of the depression center. Stippling indicates areas of continuous high cloud in the satellite infrared imagery around 1800 GMT.

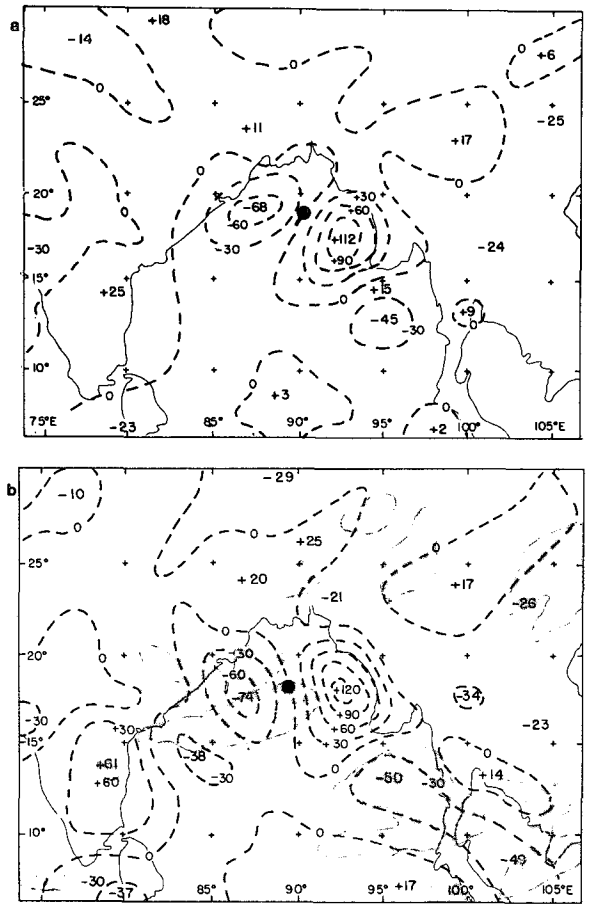

FIG. 14. As in Fig. 13 but for 6 July.

if the atmosphere is saturated on the large scale, as it apparently nearly was in this case, then this activity does not add appreciably to the large-scale average precipitation. In the present case, it is likely that the role of cumulus convection within the main rainstorm of the depression (as opposed to sporadic precipitation at large distances from it) was to provide small-scale variability in space and time. The ascent forced by quasi-geostrophic advections of temperature and vorticity in an atmosphere of nearly neutral static stability appears to have been sufficient to account for the storm-averaged rainfall, with little need for Ekman pumping or other, more exotic, mechanisms. A quasi-geostrophic prediction of a depression over land by Krishnamurti *et al.* (1976), on the other hand, produced no precipitation save that due to a convective parameterization scheme at the initial time.

6. Streamfunction tendency

With Eq. (2) solved for ω at 700 and 400 mb, the mean divergences in the lower, middle, and upper layers were obtained by simple vertical differencing. Then, a finite difference analogue of the quasi-geostrophic vorticity equation, excluding the effect of friction,

$$\nabla^2 \frac{\partial \psi}{\partial t} = -\mathbf{V} \cdot \nabla(\nabla^2 \psi + f) + f_0 \frac{\partial \omega}{\partial p} \qquad (4)$$

was solved with the streamfunction tendency set equal to zero on the lateral boundaries. Calculations were performed for sets of divergence values derived from results of each of the choices of stability and lower-boundary vertical motion as described.

Fields of streamfunction tendency for the nearly-neutral static stability value are shown in Figs. 16, 17 and 18, along with portions (near the depression center) from calculations with the full dry stability. Comparison of the two affords insight into the effects of vorticity advection and divergence $\partial\omega/\partial p$ since the latter is almost completely suppressed in the dry-stability calculations owing to the extremely small vertical motions previously discussed.

As anticipated, intensification of the depression is not indicated by any of the results. The slight positive tendency values over the center in the lower layer and the weak negative ones in the middle layer probably

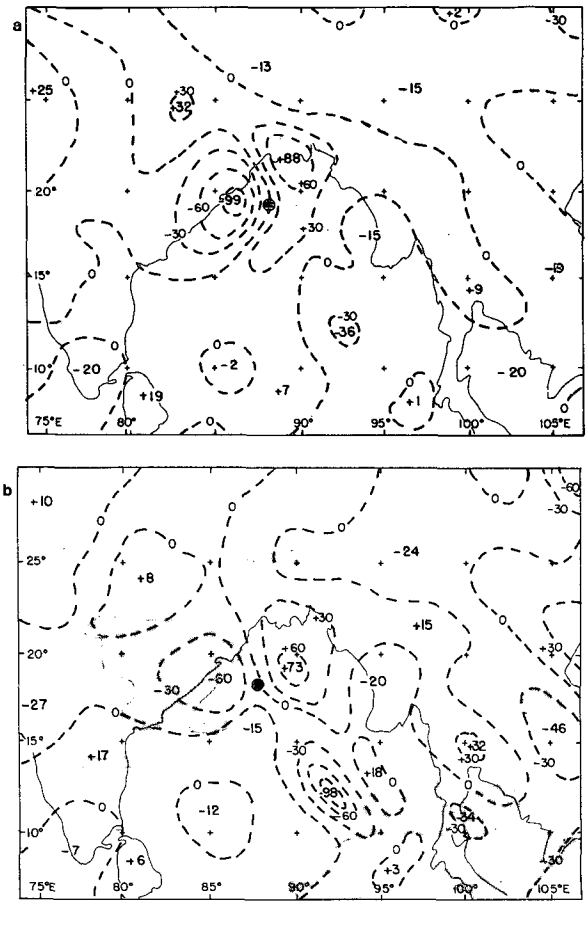

FIG. 15. As in Fig. 14 but for 7 July.

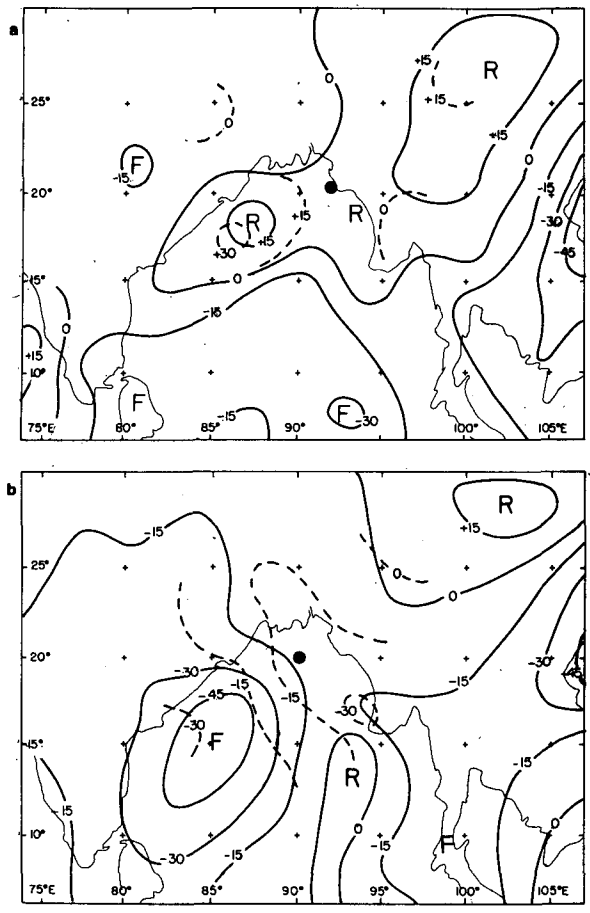

FIG. 16. Streamfunction tendency ($m^2 s^{-2}$) for σ equal to 1% of the dry-adiabatic value (solid) and to the dry adiabatic value (dashed) at 1200 GMT 5 July: (a) for the lower layer; (b) for the middle layer. Letters denoting centers of rise and fall refer to the solid isopleths. The large dot indicates the concurrent position of the streamfunction minimum.

arise from the map-average beta effect $-\mathbf{V}\cdot\nabla f$ since the average meridional components are southerly in the lower layer and northerly in the middle. The Laplacian of the tendency at both levels (a more fundamental measure of intensification than the tendency itself), in fact, is nearly zero at both levels and on all three days, since the vorticity advection is zero and the divergence, as pointed out earlier, is nearly so. In the calculations with ω_s calculated from (3), there is a large rise over the depression center, due to divergence above the ascent resulting from Ekman pumping. Thus, the quasi-geostrophic theory fails in a crucial aspect.

The motion of the depression center is a different matter. From kinematic considerations we can obtain the displacement speed C of the streamfunction minimum from

$$C = -\left[\frac{\partial}{\partial s}\left(\frac{\partial \psi}{\partial t}\right)\right]\left(\frac{\partial^2 \psi}{\partial s^2}\right)^{-1}, \qquad (5)$$

where the s-axis is chosen along the gradient of streamfunction tendency at the center, directed from rises toward falls. The direction of displacement of the center is along the s-axis. In the evaluation of C, for the tendencies based on the small stability, a mesh length equal to the one used in the main calculations was employed.

Results appear in Table 2. Comparison with the observed track of the center in Fig. 6 shows that the calculated speeds are reasonable, somewhat too slow in the middle layer and just slightly too fast in the lower layer. The observed separation of the centers in the two layers is qualitatively indicated, but exaggerated, especially on the first two days, the calculated direction of the lower-layer and middle-layer centers being too much northward and too much southward, respectively. In reality, vertical advection of vorticity over the center may act to keep the vortex relatively vertical. Westward progress in both layers is indicated on all three days, as observed.

These results, with the strong divergence effect included, are much better than those based essentially on vorticity advection (quasi-barotropic), as shown in Figs. 16, 17, and 18. By inspection it appears that the

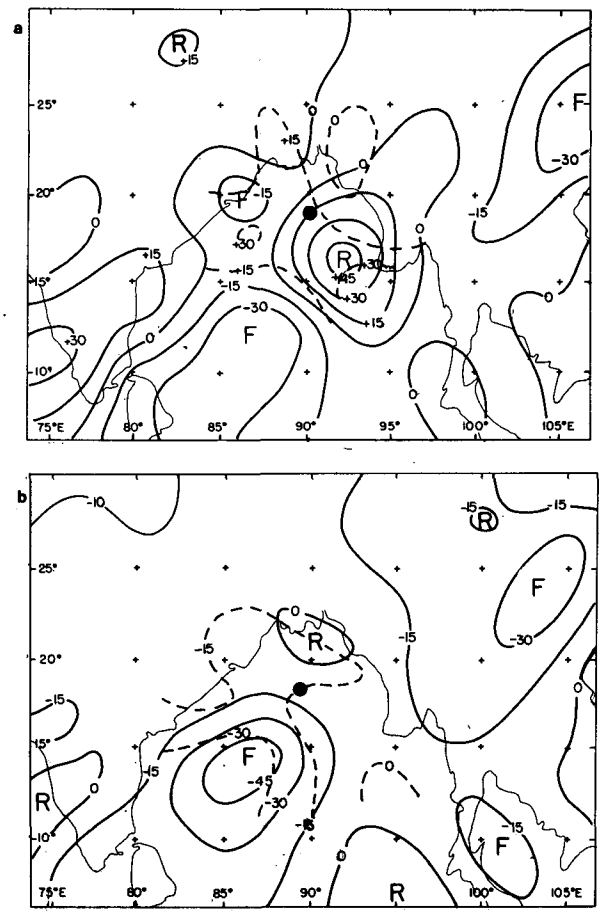

FIG. 17. As in Fig. 16 but for 6 July.

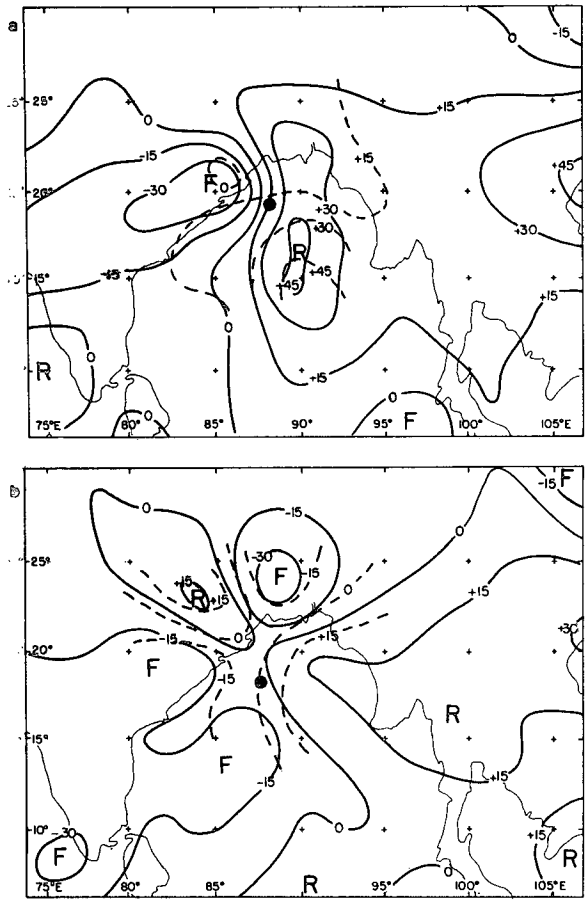

FIG. 18. As in Fig. 16 but for 7 July.

lower-layer center in the quasi-barotropic calculations is moving east-northeastward on the 5th and 6th, and north-northwestward on the 7th, nearly opposite to the observed motion on the first two days. In the middle layer, the quasi-barotropic indications are for motion toward east-southeast on the 5th, north-northwest on the 6th, and west-northwest on the 7th, again poorer than the results with strong divergence effects. This finding contrasts with that of Krishnamurti *et al.* (1976) who showed poor agreement between the observed motion and either a barotropic or a 2-level quasi-geostrophic baroclinic forecast. The difference may be attributable to the better data coverage in this case.

In summary, it seems clear that strong vertical motions are required to supply the divergence necessary to account for the displacement of the center, in agreement with the findings of Rao and Rajamani (1970). Vertical motions computed from conventional quasi-geostrophic effects acting on an atmosphere of nearly neutral stability, are apparently adequate, as the resulting errors in displacement velocity are no larger than those in predictions of other tropical and temperate systems for which the physical mechanisms are reasonably well-known, and may arise from uncertainty in specification of the flow fields.

7. Conclusions

Application of quasi-geostrophic diagnosis to this uniquely well-observed monsoon depression yields mixed results. The rapid intensification of the center between 5 and 6 July 1979 is not accounted for by the response of an atmosphere with nearly moist-adiabatic stratification to advections of temperature and vorticity. Some effect, presumably related to convergence in the surface boundary layer and similar to CISK, may produce an upward-increasing vertical motion above the top of the layer, so that growth of vorticity can occur *in situ.* Shukla (1978) has demonstrated the importance of the CISK mechanism, together with barotropic–baroclinic instability, in producing monsoon depressions. In this light it seems curious that no obvious cloud signature appears in the satellite imagery. Further, Warner (1984) found warm dry air in the center on the 7th. It is possible that the vorticity growth occurs on air parcels as they travel toward the center, rather than *in situ,* in a way that escapes quasi-geostrophic diagnosis.

TABLE 2. Calculated and observed displacement velocity of the depression center.

Date	Layer	Direction of s-axis		Displacement speed (m s^{-1})	
		Calculated	Observed	Calculated	Observed
5 July	Lower	Toward 320°		1.9	
	Middle	Toward 220°		1.4	
5–6 July	Lower		Toward 230°		2.2
	Middle		Toward 200°		2.6
6 July	Lower	Toward 310°		3.0	
	Middle	Toward 205°		1.4	
6–7 July	Lower		Toward 270°		2.4
	Middle		Toward 270°		2.6
7 July	Lower	Toward 290°		4.7	
	Middle	Toward 240°		1.9	

The westward motion of the system, once established, is accounted for much more successfully, however, provided that the large horizontal divergences associated with the nearly neutral stratification are taken into account in the vorticity equation. The discrepancies between diagnosed and observed motion, while not small compared to the observed motion, are no larger than the absolute discrepancies in dynamical prediction of other types of cyclones for which the mechanism of displacement is considered to be well-known. The small observed and diagnosed motion represents a near balance between effects of divergence and of vorticity advection. It seems curious then that the tracks of depressions are so regular, as imbalance would seem to favor more or less random dispersion. We might speculate that the mechanism of formation requires that the center will develop near the trough-line with little zonal basic current and thus very small vorticity advection, rather than within the flanking currents where steering effects would be strong. Then the motion, however small, would be dominated by divergence effects associated with the advection of the basic temperature pattern (warmer to the north, cooler to the south) by the developing cyclonic circulation.

The storm-scale ascent west of the center appears to be adequate to account for the area-averaged precipitation produced by the depression, again on the assumption of nearly neutral stratification. The role of any embedded convection in this region must then be primarily to add detail on the small temporal and spatial scales. The ascent appears to represent mainly the effect of warm advection and lies approximately due west of the mean position of the depression (averaged in depth through the lower and middle troposphere). Since the meridional slope of the depression with elevation is toward the south, the maximum ascent lies south of, as well as west of, the position of the depression at the surface. This position is consistent with the usual position of the major precipitation area relative to a monsoon depression.

The monsoon depression is thus found to be a peculiar phenomenon. It is unlike either the tropical cyclone of lower latitudes, which depends not at all on the vertical wind shear in the large-scale ambient flow (other than to avoid it), or the extratropical storm of higher latitudes which depends entirely on this vertical wind shear, or the so-called "hybrid" storm of subtropical latitudes with which it shares some characteristics but which appears to develop as an intense reaction to forcing of the type found to be ineffective in this study. Cursory examination of the data suggests that the closest resemblance may be to some of the weaker typhoons of the neighboring South China Sea.

Acknowledgments. The author is grateful to Dr. K. R. Saha for many stimulating disputations on monsoon depressions, and also to Ms. Sylvia Lanza for programming the diagnostic model. The research was supported by the National Science Foundation under Grants ATM-7823779 and ATM-8019301.

REFERENCES

Burpee, R. W., 1972: The origin and structure of easterly waves in the lower troposphere of North Africa. *J. Atmos. Sci.*, **29,** 77–90.

Charney, J. G., 1963: A note on large-scale motions in the tropics. *J. Atmos. Sci.*, **6,** 607–609.

Gates, W. L., and A. B. Nelson, 1975: A new (revised) tabulation of the Scripps topography on a 1° global grid. Part I: Terrain heights. The Rand Corporation, R-1276-1-ARPA. ARPA Order No. 189-1.

Keshavamurty, R. N., G. C. Osnani, P. V. Pillai and S. K. Das, 1978: Some studies of the growth of monsoon disturbances. *Proc. Indian Acad. Sci.*, **87A,** 61–75.

Krishnamurti, T. N., M. Kanamitsu, R. Godbole, C. B. Chang, F. Carr and J. H. Chao, 1976: Study of a monsoon depression (II), dynamical structure. *J. Meteor. Soc. Japan,* **54,** 208–225.

Newell, R. E., J. W. Kidson, D. G. Vincent and G. J. Boer, 1972: *The General Circulation of the Tropical Atmosphere.* The MIT Press, 258 pp.

Nitta, T., and K. Masuda, 1981: Observational study of a monsoon depression developed over the Bay of Bengal during Summer MONEX. *J. Meteor. Soc. Japan,* **59,** 672–682.

Raman, C. R. V., Y. P. Rao, S. K. Subramanian and Z. E. Sheikh, 1978: Wind shear in a monsoon depression. *Nature,* **275,** 51–53.

Rao, K. V., and Rajamani, 1970: Diagnostic study of a monsoon depression by geostrophic baroclinic model. *Indian J. Meteor. Geophys.*, **21,** 187–194.

Rao, Y. P., 1976: Southwest Monsoon. *Meteor. Monogr. Synoptic Meteor.*, No. 1. Indian Meteor. Dept., New Delhi, 107–185.

Saha, K. R., and S. S. Singh, 1972: On the distribution of mean static stability and mean Richardson number in the tropical atmosphere. *J. Meteor. Soc. Japan,* **50,** 313–323.

——, F. Sanders and J. Shukla, 1981: Westward-moving predecessors of monsoon depressions. *Mon. Wea. Rev.*, **109,** 330–343.

Sanders, F., 1971: Analytic solutions of the nonlinear omega and vorticity equations for a structurally simple model of disturbances in the baroclinic westerlies. *Mon. Wea. Rev.*, **99,** 393–408.

——, and R. W. Burpee, 1968: Experiments in barotropic hurricane track forecasting. *J. Appl. Meteor.*, **7,** 313–323.

Shukla, J., 1978: CISK-barotropic-baroclinic instability and the growth of monsoon depressions. *J. Atmos. Sci.*, **35,** 494–508.

Sumner, E. J., 1950: The significance of vertical stability in synoptic development. *Quart. J. Roy. Meteor. Soc.*, **76,** 384–397.

Warner, C., 1984: Core structure of a Bay of Bengal monsoon depression. Submitted to *J. Atmos. Sci.*

World Meteorological Organization, 1981: Summer MONEX Field Phase Report, FGGE Operations Report, Vol. 8, 179 pp.

Young, J. A., H. Virji, D. P. Wylie and C. Lo, 1980: Summer monsoon windsets from geostationary satellite data, Summer MONEX, 1 May–31 July 1979. Space Sci. and Eng. Center and Dept. of Meteor., University of Wisconsin–Madison.